J|A|C|S
ARTICLES
Published on Web 03/18/2006

Assemblies of Supramolecular Porphyrin Dimers in Pentagonal and Hexagonal Arrays Exhibiting Light-Harvesting Antenna Function

Fatin Hajjaj,[†] Zin Seok Yoon,[‡] Min-Chul Yoon,[‡] Jaehong Park,[‡] Akiharu Satake,[†] Dongho Kim,*[,‡] and Yoshiaki Kobuke*[,†]

Contribution from the Graduate School of Materials Science, Nara Institute of Science and Technology, Takayama 8916-5, Ikoma, Nara 630-0192, Japan, and Department of Chemistry and Center for Ultrafast Optical Characteristics Control, Yonsei University, Seoul 120-749, Korea

Received December 7, 2005; E-mail: dongho@yonsei.ac.kr; kobuke@ms.aist-nara.ac.jp

Abstract: Porphyrin-based supramolecular macrocyclic arrays were synthesized as mimics of photosynthetic light-harvesting (LH) antennae. Pentameric and hexameric macrocyclic porphyrin arrays **EP5** and **EP6** were constructed by complementary coordination of *m*-bis(ethynylene)phenylene-linked zinc-imidazolylporphyrin **Zn-EP-Zn**. The proton NMR spectra of noncovalently linked **N-EP5** and **N-EP6** indicate fast rotation of the porphyrin moieties along the ethyne axis. These macrocycles were covalently linked and identified as **C-EP5** (6832 Da) and **C-EP6** (8199 Da) by mass spectrometry. Fluorescence quantum yields of **C-EP2** (10.0%), **C-EP5** (10.1%), and **C-EP6** (11.0%), even larger than that of the unit coordination dimer **C-EP1** (9.3%), were significantly increased from those of the series without the ethynylene linkage. The order of increasing fluorescence quantum yields was parallel to that of decreasing fluorescence lifetimes (**C-EP1** (1.65 ns), **C-EP2** (1.45 ns), **C-EP5** (1.42 ns), and **C-EP6** (1.38 ns)), indicating that the radiative decay rate k_F increased relative to the other decay rates with an increase in the number of ring components. Based on the exciton−exciton annihilation and anisotropy depolarization times, the excitation energy hopping (EEH) times in these macrocyclic systems were obtained as 21 ps for **C-EP5** and 12.8 ps for **C-EP6**. EEH times depend strongly on the orientation factor of the component transition dipoles in the macrocyclic arrays. The hexagonal macrocyclic array with an orientation of better transition dipole coupling resulted in faster EEH time compared to the pentagonal one.

Introduction

Photosynthetic light-harvesting (LH) antennae are efficient molecular devices for catching dilute sunlight energy and transferring the excitation energy to the reaction center through an antenna network. Purple bacteria adopt macrocyclically the LH systems LH1 and LH2, in which, respectively, 30 and 16 bacteriochlorophylls (BChls) are arranged in circular arrays.[1] Circular structures are favored in forming densely packed two-dimensional arrays in biological membranes.[2] They are effective in absorbing light from any direction due to the isotropic nature of the circle and in transferring the energy to neighboring antenna molecules in the ring and further to other rings by excited energy hopping (EEH) processes.

Synthetic models of LH antennae without the protein matrix are useful for exploring photochemical solar energy conversion and other optoelectronic devices operating at the molecular level. Porphyrin-based LH antennae have been investigated thoroughly due to their close relation to the chlorophyll system with respect to structure and photophysical properties.[3] The fabrication and characterization of macrocyclic porphyrin arrays to resemble LH complexes in purple bacteria, however, are rather limited. So far, the researches on a diphenylbutadiyne-linked cyclic tetramer,[4] *m*-bis(phenylethynyl)phenylene-linked cyclic hexamer,[5] and diphenylethyne-linked cyclic hexamer[6] have been reported. Recently, *m*-phenylene- and *meso-meso*-linked cyclic dodecamers, in which 12 porphyrins are closely connected, were reported to exhibit fast EEH.[7]

Self-assembling into macrocyclic porphyrin arrays through noncovalent bonds is challenging from a viewpoint of synthetic accessibility to nature's methodology. Cyclic tetramers using hydrogen bonds[8] and cyclic dodecamers formed through axial coordination of substituted pyridines to six-coordinated cobalt

[†] Nara Institute of Science and Technology.
[‡] Yonsei University.

(1) (a) Hu, X.; Damjanović, A.; Ritz, T.; Schulten, K. *Proc. Natl. Acad. Sci. U.S.A.* **1998**, *95*, 5935−5941. (b) Green, B. R., Parson, W. W., Eds. *Light-Harvesting Antennas in Photosynthesis*; Advances in Photosynthesis and Respiration series, Vol. 13; Kluwer Academic Publishers: Dordrecht, The Netherlands, 2003. (c) McDermott, G.; Prince, S. M.; Freer, A. A.; Hawthornthwaite-Lawless, A. M.; Papiz, M. Z.; Cogdell, R. J.; Isaacs, N. W. *Nature* **1995**, *374*, 517−521. (d) Koepke, J.; Hu, X.; Muenke, C.; Schulten, K.; Michel, H. *Structure* **1996**, *4*, 581−597. (e) Roszak, A. W.; Howard, T. D.; Southall, J.; Gardiner, A. T.; Law, C. J.; Isaacs, N. W.; Cogdell, R. J. *Science* **2003**, *302*, 1969−1972.
(2) (a) Scheuring, S.; Sturgis, J. N.; Prima, V.; Bernadac, A.; Lévy, D.; Rigaud, J.-L. *Proc. Natl. Acad. Sci. U.S.A.* **2004**, *101*, 11293−11297. (b) Bahatyrova, S.; Frese, R. N.; Siebert, C. A.; Olsen, J. D.; van der Werf, K. O.; van Grondelle, R.; Niederman, R. A.; Bullough, P. A.; Otto, C.; Hunter, C. N. *Nature* **2004**, *430*, 1058−1062.

 10.1021/ja0583214 CCC: $33.50

porphyrins[9] have been demonstrated. Although the latter structurally resembles natural LH2, no LH function is expected from nonfluorescent cobalt porphyrins.

We have recently developed a complementary coordination of bis(zinc-imidazolylporphyrin) to construct macrocyclic porphyrin arrays.[10] When two zinc-imidazolylporphyrins are linked with an appropriate spacer, various macrocyclic porphyrin arrays can be obtained in good yields. In the coordination dimer (hereafter called as "dimer"), two porphyrins form a slipped-cofacial structure, like the chlorophyll dimer in LH2, and EEH in the dimer occurs very rapidly on a subpicosecond time scale.[11] In the macrorings, a different EEH process across the covalently connected spacer was observed.

Previously, we reported the first macrocyclic pentamer **P5** and hexamer **P6** supramolecules from bis(zinc-imidazolylporphyrin) linked through a *m*-phenylene moiety.[10a,11] In these rings, because porphyrin and phenylene planes are orthogonal to each other, the π-conjugation between porphyrins is prohibited. In the present work, we have explored the supramolecular formation of the cyclic pentamer **EP5** and hexamer **EP6** from bis(zinc-imidazolylporphyrin) linked by a *m*-bis(ethynyl)phenylene spacer. Introduction of the ethyne moiety between porphyrin and phenylene allows free rotation along the ethyne axis, and an intimate electronic communication among porphyrins would occur as a result of the coplanar conformation. In addition, the transition dipole of porphyrin along the axis of π-conjugation is increased, as observed for the red-shift and increased intensity of the Q-bands, otherwise symmetry forbidden. In natural LH systems, vectorial energy flow is realized by arranging multiple LH units, such as LH2 and LH1 in purple bacteria. In this context, **EP5** and **EP6** can be potential candidates for accepting high-excitation energy from **P5** and **P6**.

Here, we report the efficient synthesis of noncovalently linked **N-EP5** and **N-EP6** and covalently linked **C-EP5** and **C-EP6**. Their dynamic behaviors are examined by ^{1}H NMR, and LH antenna functions are evaluated by steady-state absorption, emission, and time-resolved transient absorption techniques. We compare the LH functions with those of **P5** and **P6** and discuss the effect of ring size and orientation factor in the EEH process.

Results

Synthesis of N-EP5, N-EP6, C-EP5, and C-EP6. We have examined the self-assembly of macrocyclic porphyrin arrays from various bis(zinc-imidazolylporphyrin)s. If an appropriate bisporphyrin unit is prepared, the desired porphyrin array can be produced in good yields by the reorganization technique. **EP5** and **EP6** require the bisporphyrin unit **Zn-EP-Zn**. In our first attempt at preparing **Zn-EP-Zn**, the double Sonogashira coupling[12] of 1,3-diiodo-benzene with porphyrin **2** was examined. When porphyrin **2** (2 equiv) and 1,3-diiodo-benzene (1 equiv) were reacted in the presence of the catalyst $Pd_2(dba)_3$/$AsPh_3$, the desired **H_2-EP-H_2** was obtained along with **4**, **H_2-EP**, and **H_2-3** with the recovery of **2**. Oxidative coupling product **4** generally accompanies the palladium catalyzed coupling reaction of ethynylporphyrins. Unfortunately, **H_2-EP-H_2** could not be separated from **4** effectively by various chromatographical techniques (SiO_2, Al_2O_3, and GPC) owing to the similarity of polarities and molecular volumes. Finally, we have established the synthetic scheme for **Zn-EP-Zn** shown in Scheme 1. First, the monocoupling product **H_2-3** was prepared in 78% yield from **2** with an excess 1,3-diiodo-benzene in the presence of the catalyst $Pd_2(dba)_3$/$AsPh_3$. After zinc insertion into **H_2-3**, the coupling reaction of **Zn-3** with **2** gave **H_2-EP−Zn** as the dominant product along with **H_2-EP** and **4**. This time, **H_2-EP-Zn** was isolated successfully in 50% yield by gel permeation chromatography. **H_2-EP** was also isolated in 10% yield, and its zinc complex **Zn-EP** was used as a reference compound for steady state and transient absorption measurements.

Zinc insertion into **H_2-EP-Zn** afforded the bis-zinc complex **Zn-EP-Zn**, which spontaneously organized into oligomers by the complementary coordination of imidazolyl residues to zinc centers.[13] GPC analysis of the as-prepared (pristine) **Zn-EP-Zn** oligomers showed a broad molecular weight distribution with sharp spikes at longer retention times (Figure S1, red curve). The pattern of the first chromatogram was close to those obtained in the cases of **P5** and **P6**,[10a] suggesting that the formation of specific cyclic oligomers was accompanied by the formation of a significant amount of linear oligomers.

To dominate the intramolecular cyclization, the **Zn-EP-Zn** oligomeric mixture was reorganized as follows. A 20.0 μM solution of the mixture was prepared in $CHCl_3$/MeOH = 10/1 (v/v), and the solution was allowed to stand at rt for 1 day. During this period, conversion into **N-EP5** and **N-EP6** proceeded in good yield. The solvents were then evaporated at 26 °C under reduced pressure as quickly as possible. The evaporation process must be controlled carefully. During the concentration process, the solvent becomes methanol-rich, and the dimer tends to dissociate. The cyclic assemblies dissociated are transformed into polymeric assemblies at higher concentra-

(3) (a) Harvey, P. D. In *The Porphyrin Handbook*; Kadish, K. M., Smith, K. M., Guilard, R., Eds.; Academic Press: New York, 2003; Vol. 18, pp 63−250. (b) Kim, D.; Osuka, A. *Acc. Chem. Res.* **2004**, *37*, 735. (c) Holten, D.; Bocian, D. F.; Lindsey, J. S. *Acc. Chem. Res.* **2002**, *35*, 57−69. (d) Choi, M.-S.; Yamazaki, T.; Yamazaki, I.; Aida, T. *Angew. Chem., Int. Ed.* **2004**, *43*, 150−158. (e) Imahori, H. *J. Phys. Chem. B* **2004**, *108*, 6130−6143. (f) Satake, A.; Kobuke, Y. *Tetrahedron* **2005**, *61*, 13−41. (g) Balaban, T. S. *Acc. Chem. Res.* **2005**, *38*, 612−623. (h) Prathapan, S.; Johnson, T. E.; Lindsey, J. S. *J. Am. Chem. Soc.* **1993**, *115*, 7519−7520. (i) Nakano, A.; Osuka, A.; Yamazaki, I.; Yamazaki, T.; Nishimura, Y. *Angew. Chem., Int. Ed. Engl.* **1995**, *34*, 1096. (j) Maruo, N.; Uchiyama, M.; Kato, T.; Arai, T.; Akisada, H.; Nishino, N. *Chem. Commun.* **1999**, 2057. (k) Yeow, E. K. L.; Ghiggino, K. P.; Reek, J. N. H.; Crossley, M. J.; Bosman, A. W.; Schenning, A. P. H. J.; Meijer, E. W. *J. Phys. Chem. B* **2000**, *104*, 2596−2606. (l) Choi, M.-S.; Aida, T.; Yamazaki, T.; Yamazaki, I. *Angew. Chem., Int. Ed*. **2001**, *40*, 3194. (m) Aratani, N.; Osuka, A.; Kim, Y. H.; Jeong, D. H.; Kim, D. *Angew. Chem., Int. Ed.* **2000**, *39*, 1458. (n) Ogawa, K.; Kobuke, Y. *Angew. Chem., Int. Ed.* **2000**, *39*, 4070. (o) Furutsu, D.; Satake, A.; Kobuke, Y. *Inorg. Chem.* **2005**, *44*, 4460−4462. (p) Drain, C. M.; Goldberg, I.; Sylvain, I.; Falber, A. *Top. Curr. Chem.* **2005**, *245*, 55. (q) You, C.-C.; Dobrawa, R.; Saha-Möller, C. R.; Würthner, F. *Top. Curr. Chem.* **2005**, *258*, 39.
(4) Anderson, S.; Anderson, H. L.; Bashall, A.; McPartlin, M.; Sanders, J. K. *Angew. Chem., Int. Ed. Engl.* **1995**, *34*, 1096−1099.
(5) Mongin, O.; Schuwey, A.; Vallot, M.-A.; Gossauer, A. *Tetrahedron Lett.* **1999**, 40, 8347.
(6) Tomizaki, K.-Y.; Yu, L.; Wei, L.; Bocian, D. F.; Lindsey, J. S. *J. Org. Chem.* **2003**, *68*, 8199−8207.
(7) (a) Hwang, I.-W.; Ko, D. M.; Ahn, T. K.; Yoon, Z. S.; Kim, D.; Peng, X.; Aratani, N.; Osuka, A. *J. Phys. Chem. B* **2005**, *109*, 8643−8651. (b) Peng, X.; Aratani, N.; Takagi, A.; Matsumoto, T.; Kawai, T.; Hwang, I.-W.; Ahn, T. K.; Kim, D.; Osuka, A. *J. Am. Chem. Soc.* **2004**, *126*, 4468−4469.
(8) Shi, X.; Barkigia, K. M.; Fajer, J.; Drain, C. M. *J. Org. Chem.* **2001**, *66*, 6513−6522.
(9) Haycock, R. A.; Hunter, C. A.; James, D. A.; Michelsen, U.; Sutton, L. R. *Org. Lett.* **2000**, *2*, 2435−2438.
(10) (a) Takahashi, R.; Kobuke, Y. *J. Am. Chem. Soc.* **2003**, *125*, 2372−2373. (b) Ikeda, C.; Satake, A.; Kobuke, Y. *Org. Lett.* **2003**, *5*, 4935−4938. (c) Kuramochi, Y.; Satake, A.; Kobuke, Y. *J. Am. Chem. Soc.* **2004**, *126*, 8668−8669. (d) Shoji, O.; Okada, S.; Satake, A.; Kobuke, Y. *J. Am. Chem. Soc.* **2005**, *127*, 2201−2210. (e) Takahashi, R.; Kobuke, Y. *J. Org. Chem.* **2005**, *70*, 2745−2753.
(11) Kim, D.; Miyasaka, H.; Kobuke, Y.; et al. *Chem.−Eur. J.* **2005**, *11*, 3753.
(12) Sonogashira, K.; Tohda, Y.; Hagihara, N. *Tetrahedron Lett.* **1975**, *16*, 4467−4470.
(13) Kobuke, Y.; Miyaji, H. *J. Am. Chem. Soc.***1994**, *116*, 4111−4112.

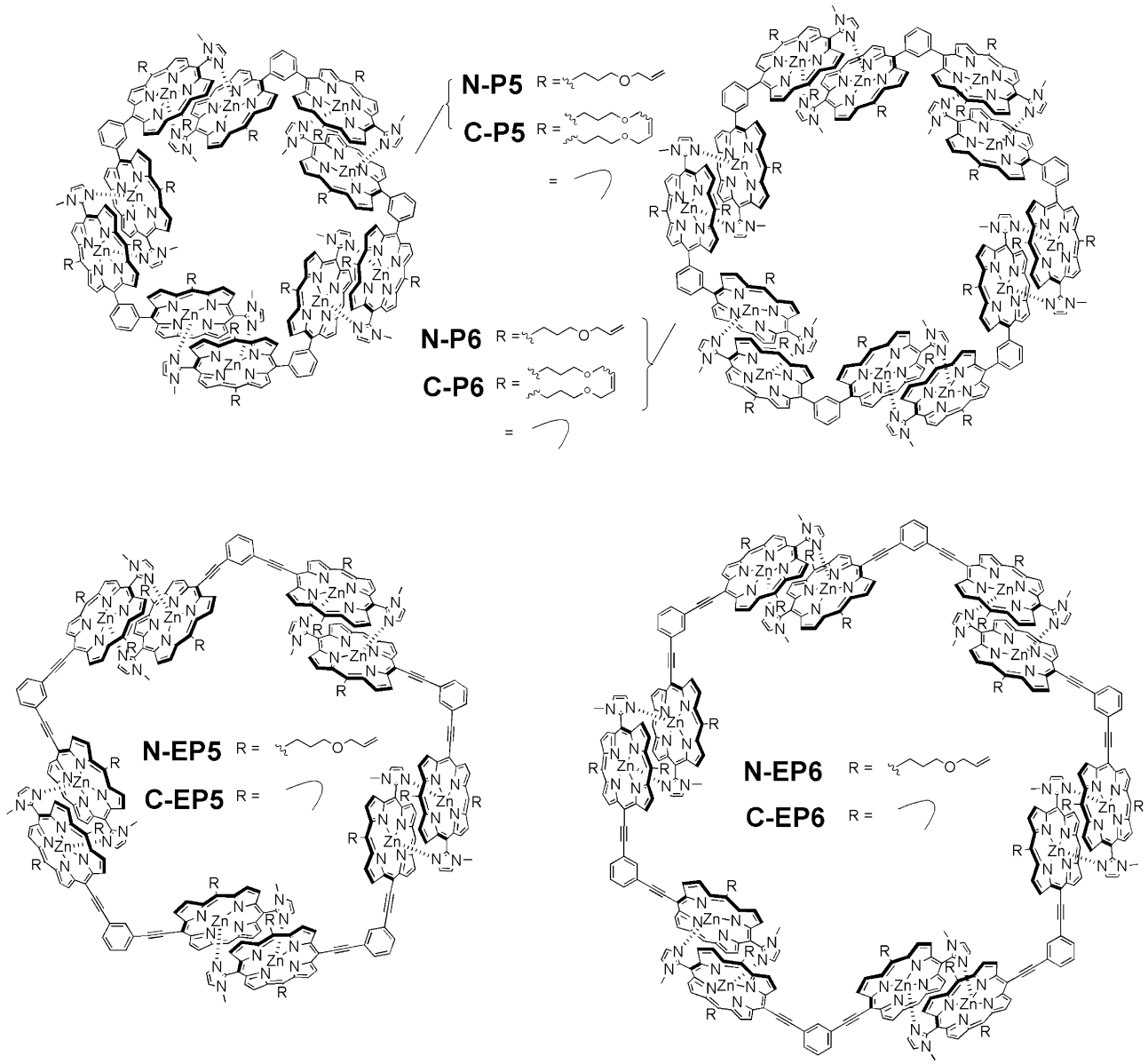

Figure 1. Structures of macrocyclic porphyrin arrays.

tions.[10a,d,e,14] Evaporation under these circumstances increases the amount of oligomer and, thus, must be performed quickly. The use of large volumes should be avoided for a reason. An analytical GPC trace of the sample reorganized from **Zn-EP-Zn** (Figure S1, blue curve) showed two converged peaks, putative cyclic hexamer and pentamer **N-EP6** and **N-EP5**, respectively, and the higher molecular weight components disappeared. **N-EP6** and **N-EP5** were separated using preparative GPC, and their purities were checked by analytical GPC (Figure S2).

The isolated components are stable in solid form and in noncoordinating solvents such as $CHCl_3$ ($\sim$10 μM) and toluene. The dimer units in the isolated assemblies were covalently linked by olefin metathesis reactions. Each covalently linked macroring was purified by preparative GPC with $CHCl_3$/MeOH (10/1) as eluent, and its purity was checked by analytical GPC (Figure S3). The metathesis reaction enables the detection of molecular ion peaks of *m*/*z* 6832 and 8199, corresponding to the covalently linked pentamer **C-EP5** and hexamer **C-EP6**, respectively. Covalent linkage also allows photophysical measurements even in coordinating solvents such as pyridine.[15] As reference molecules, porphyrins **C-EP1** and **C-EP2** were prepared by mixing **Zn-EP** and **Zn-EP-Zn** in pyridine followed by evaporation and metathesis reaction. **C-EP1** and **C-EP2** were isolated by recycling GPC (Figure S6).

Structural Analysis by ^{1}H NMR. Proton NMR analysis of **N-EP5**, **N-EP6**, **H_2-3**, and **Zn-3** was carried out in $CDCl_3$ at 25 °C (Figure 3). Under these conditions, zinc-imidazolylporphyrin exists solely as a dimer. Protons Im_5, Im_4, *N*-Me, β_1, and β_2 of **Zn-3** are upfield shifted considerably to 5.51, 2.09, 1.69, 5.42, and 8.90 ppm, respectively, compared to the corresponding peaks of **H_2-3**. By contrast, β_3 and β_4 protons of **Zn-3** are downfield shifted as a result of the deshielding effect.

(14) (a) Chi, X.; Guerin, A. J.; Haycock, R. A.; Hunter, C. A.; Sarson, L. D. *J. Chem. Soc., Chem. Commun.* **1995**, 2563. (b) Ercolani, G. *J. Phys. Chem. B* **1998**, *102*, 5699.

(15) Ohashi, A.; Satake, A.; Kobuke, Y. *Bull. Chem. Soc. Jpn.* **2004**, *77*, 365−374.

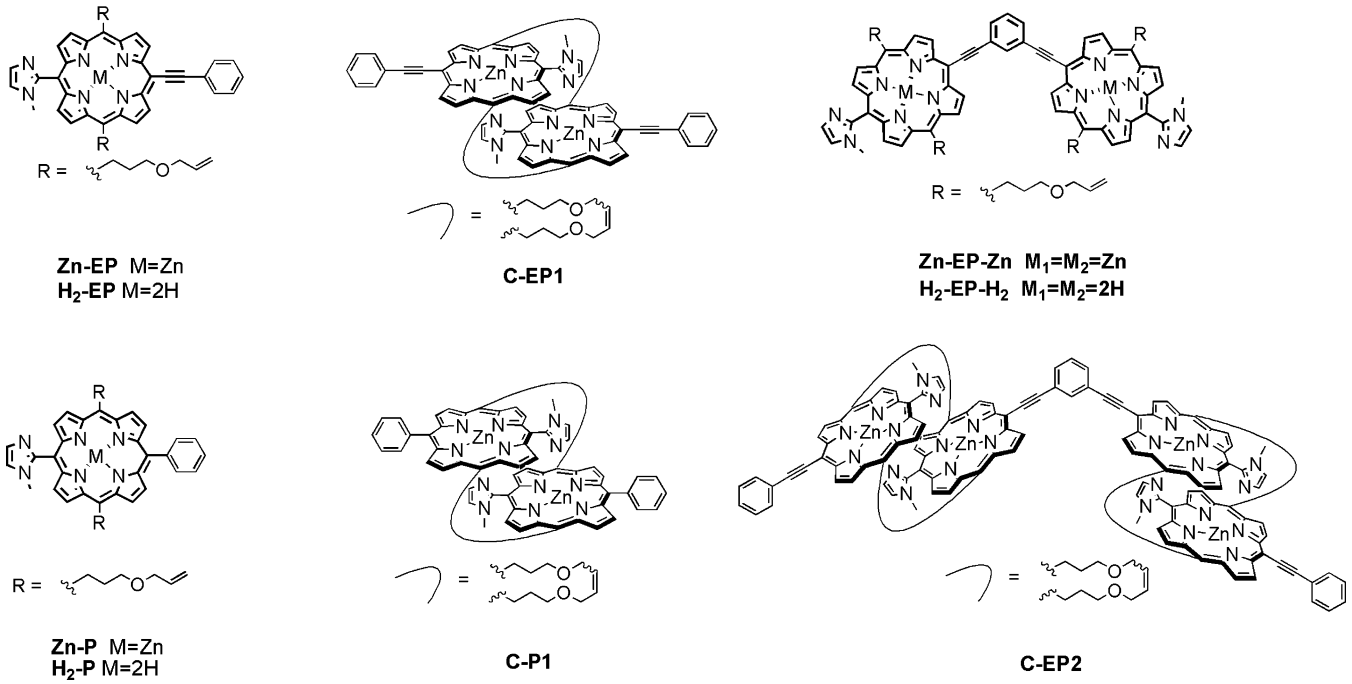

Figure 2. Structures of reference porphyrins.

Scheme 1. Synthetic Scheme of **H_2-EP-Zn**

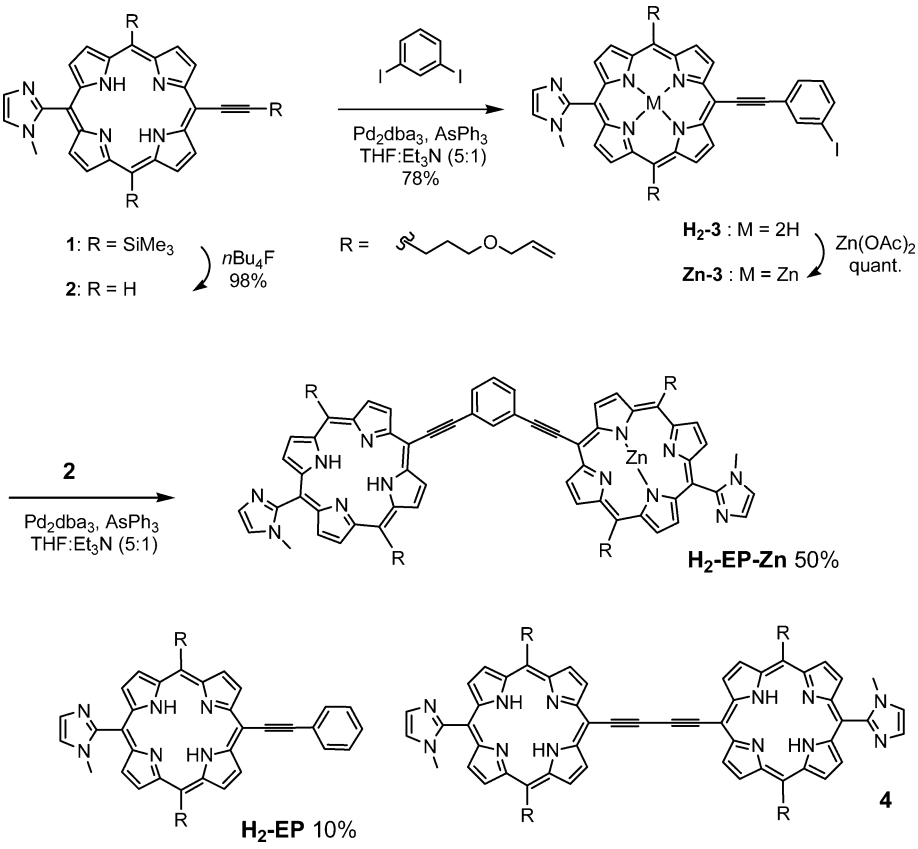

This behavior is consistent with the previous observations of zinc imidazolylporphyrin dimer.[15]

Surprisingly, both **N-EP5** and **N-EP6** gave well-resolved ^{1}H NMR spectra. The spectra exhibited only a single set of porphyrin protons, which resembles that of the starting dimer **Zn-3** except for more downfield shifted aromatic protons. Similar upfield shifts of Im_5, Im_4, *N*-Me, β_1, and β_2 protons of **N-EP5** and **N-EP6** support the formation of the dimer, and the simplicity of ^{1}H NMR suggests that all 10 or 12 porphyrins are identical under the NMR conditions. Thus, inner and outer protons of the macrocyclic arrays could not be discriminated. Larger downfield shifts of phenylene protons H_a and H_c can be reasonably explained by the doubly deshielding effect of both sides of the dimers. The chemical shifts of H_a and H_c in,

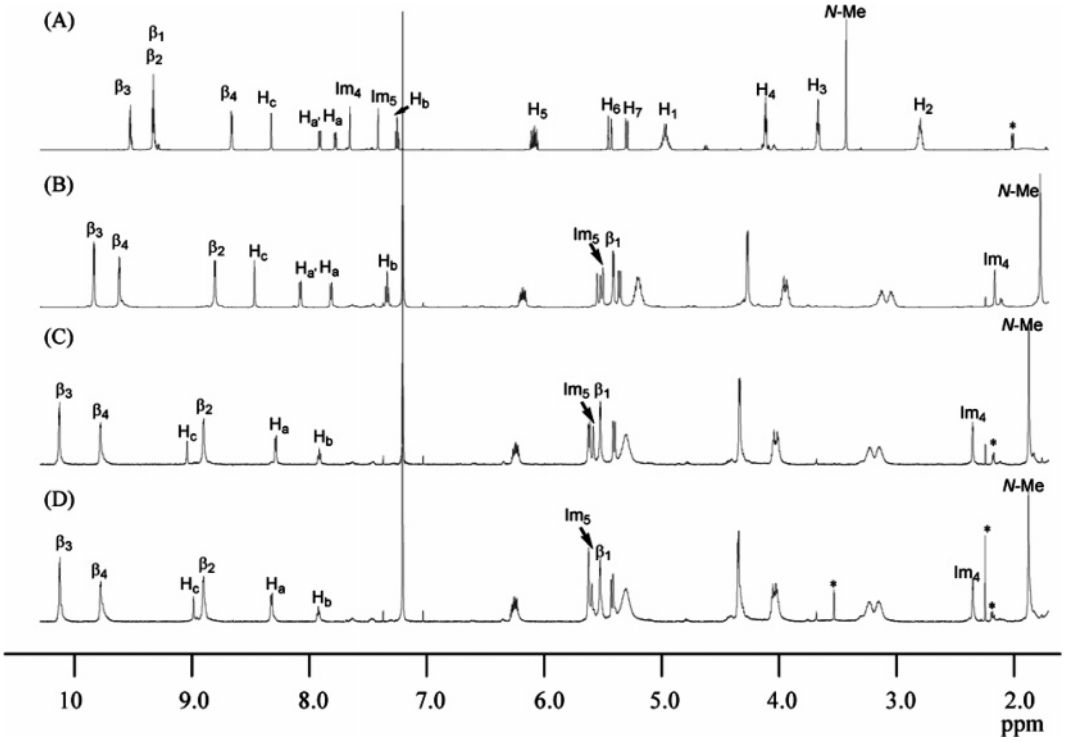

Figure 3. ^{1}H NMR spectra of (A) **H_2-3**, (B) **Zn-3**, (C) **N-EP5**, and (D) **N-EP6** in $CDCl_3$ at 25 °C. Asterisk (*) indicates impurity signals. Assignments are indicated in Figure 4.

Scheme 2. Synthetic Scheme of **C-EP5** and **C-EP6**

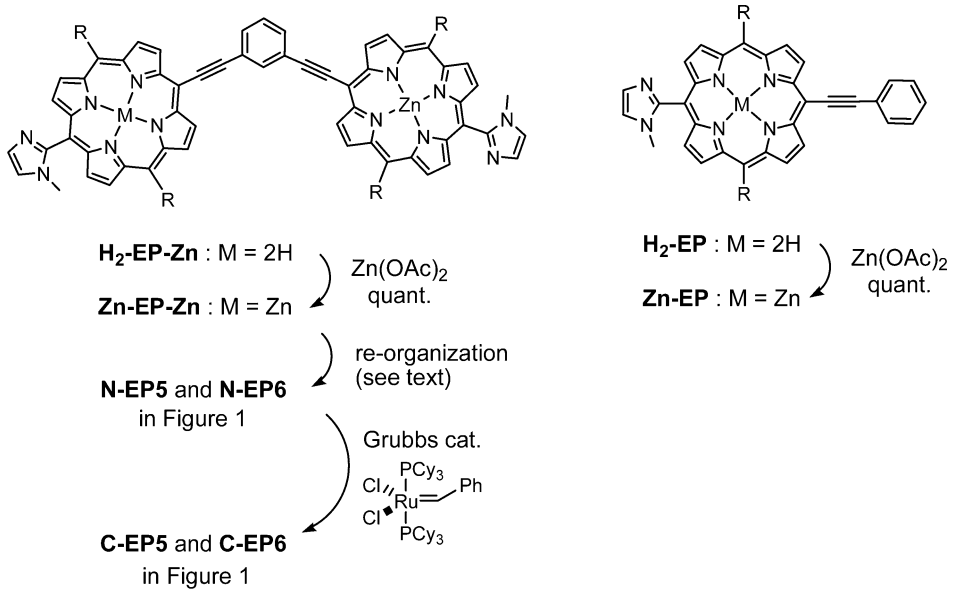

respectively, **N-EP5** and **N-EP6** indicate the high sensitivity to spatial positions of the neighboring porphyrins. The slightly larger downfield shift of H_c (9.12 ppm) observed in **N-EP5** relative to that of **N-EP6** (9.07 ppm) can be ascribed to the stronger deshielding effect due to the smaller angle of the pentagonal structure of **N-EP5**. On the other hand, proton H_a in **N-EP5** appears at a slightly upfield position (8.35 ppm) compared to 8.38 ppm for **N-EP6**. The shift behaviors of H_c and H_a protons are reasonably understandable on the basis of the pentagonal and hexagonal geometries.

The observed ^{1}H NMR spectra in Figure 3C and D sharply contrast with those of macrocyclic porphyrin arrays of zinc-imidazolylporphyrins connected by sterically hindered spacers.[10c] In the latter case, the inner and outer protons of the macrocyclic arrays in the barrel form were discriminated because the inner protons were more shielded by the ring current effect of nearby porphyrins. Topological isomers were also observed with respect to the coordination manner, indicating a slow exchange rate, if any, among the isomers. By contrast, the dimer units in **N-EP5** and **N-EP6** were rotating fast on the NMR time scale along the ethyne axis. Given that no noticeable changes were observed in the NMR spectra at −50 °C in $CDCl_3$, the rotational barrier is presumably small even at −50 °C.

Steady-State Absorption, Fluorescence, and Fluorescence Excitation Anisotropy. The steady-state absorption spectra of macrocyclic porphyrin arrays were measured in pyridine and

Table 1. Absorption and Fluorescence Spectral Data

		absorption				fluorescence			
sample	solvent[a]	soret/nm			*Q*(0,0)/nm	*Q*(0,0) emission[b] λ_{max}/nm	Stokes shift cm^{-1}	quantum yield[b,c] Φ_F	lifetime[d] τ/ns
Zn-EP	Py	433.6		445.8	640.6	650.4	235	0.083	
C-EP1	Py	433.6		453.6	651.8	656.6	112	0.093	1.65
Zn-EP-Zn	Py			450.2	646.8	653.4	156	0.100	
C-EP2	Py	431	450	458.5	656.5	660.8	99	0.100	1.45
C-EP5	Py	431	443	460.6	659.0	663.0	92	0.101	1.42
C-EP6	Py	431	443	461.4	659.4	663.2	88	0.110	1.38
Zn-P	Py		431.8		612.4				
C-P1	Py	415.8		440.0	621.8				
C-P5[e]	Py	410	425	447	621	626.5		0.035[f]	2.18
C-P6[e]	Py	410	425	449	622	627		0.035[f]	2.19
Zn-EP[g]	Tol	433.5		451.5	649.5	654.8	124.6	0.093	
C-EP2	Tol	433.5		458.5	655	658.8	88	0.095	
N-EP5	Tol	431.5	442.5	459.0	656.5	659.2	62.4	0.095	
N-EP6	Tol	431	442	460.5	657	659.4	55	0.100	

[a] Py: pyridine. Tol: toluene. [b] Excited at 430 nm. [c] ZnTPP in pyridine (Φ_F =0.038) was used as reference [ref 18]. [d] The λ_{ex} = 420 nm and λ_{em} = 650 nm were applied for the isotropic fluorescence measurement. The fluorescence lifetimes were obtained by averaging the fitted parameters measured in several emission wavelengthe (Figure 10). [e] Reference 11. [f] Data for **N-P5** and **N-P5** in toluene [ref 10e]. [g] Coordination dimer is formed.

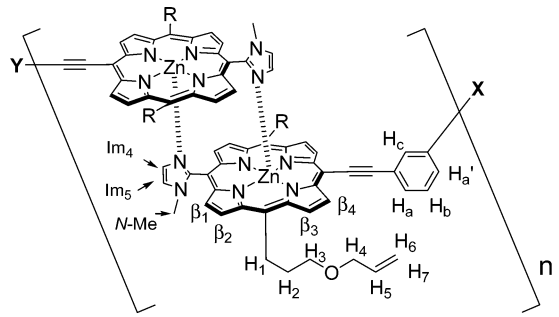

Zn-3 dimer: X = I, Y = 3-I-C_6H_4-, n=1
N-EP5: X - Y, n= 5
N-EP6: X - Y, n= 6

Figure 4. Protons assigned in Figure 3.

toluene. The absorption peaks of Soret- and Q-bands are listed in Table 1. In pyridine, noncovalently linked dimers were dissociated into monomeric species, and the absorption spectra of **Zn-EP** and **Zn-P** in pyridine represent the corresponding monomeric species with axial pyridyl coordination. In contrast, the covalently linked arrays **C-EP1**, **C-EP2**, **C-P1**, **C-EP5**, and **C-EP6** maintain their complementary coordinated structures.[15] Because of the low solubility of **C-EP6** in other common solvents, pyridine was chosen to compare the whole series of cyclic and noncyclic porphyrins. In toluene, the complementary coordination structure is perfectly maintained even without covalent linking. Since the self-association constant of the dimer unit reaches 10^{11} M^{-1} in $CHCl_3$, the coordination structure is dominant even in micromolar concentration without covalent linking.

Figure 5 compares the absorption spectra of phenylethynyl- and phenylporphyrins, **Zn-EP**, **C-EP1**, **Zn-P**, and **C-P1**. In monomeric **Zn-P**, the two transition dipoles B_x and B_y in the porphyrin plane are degenerate to show one strong Soret band at 431.8 nm. By contrast, monomeric **Zn-EP** shows two Soret bands at 433.6 and 445.8 nm due to the presence of nondegenerate B_x and B_y transition dipoles. The absorption intensity of B_x at the longer wavelength (445.8 nm), B_x, is much larger. The relative intensity of the Q(0,0) band of **Zn-EP** increases as compared to that of **Zn-P**. When the dimer (**C-EP1**) is formed, only the lower energy band is red-shifted by 7.8 nm, whereas the higher energy band remains at the same wavelength. This behavior sharply contrasts with that shown by **C-P1**, in which the degenerate Soret band (431.8 nm) splits into two bands at 415.8 and 440.0 nm due to excitonic dipole−dipole coupling by slipped-cofacial coordination as indicated in Figure 5b. The negligible blue-shift in the case of **C-EP1** may reflect the small oscillator strength of B_y.[16]

Absorption spectra of **Zn-EP-Zn**, **C-EP1**, **C-EP2**, **C-EP5**, and **C-EP6** recorded in pyridine and **Zn-EP**, **N-EP5**, and **N-EP6** recorded in toluene are shown in Figure 6. Molar extinction coefficients of the series **C-EP1**−**C-EP6** are approximately proportional to the increasing number of dimer units. The absorption spectrum of **Zn-EP-Zn** (Figure 6a, dashed-double-dotted line) shows a broad Soret band caused by through-space excitonic coupling between two porphyrin units via a *m*-phenylene spacer. The shape of the spectrum resembles those of similar bisporphyrins reported previously.[17] In the case of **C-EP2**, three Soret bands were observed at 431, 450, and 458.5 nm. The split bands (450 and 458.5 nm) can be ascribed to the dipole−dipole interaction between two dimers as shown in Figure 7. Thus, the interaction between two dipoles of two dimers produces the new integrated dipoles X (red-shift) and Y (blue-shift). The lowest energy Soret band and the Q(0,0) band are red-shifted considerably by the interaction. Further red-shifts of these bands are observed in the case of the macrocyclic arrays **C-EP5** and **C-EP6** due to the interaction with two adjacent dimers.

The steady-state fluorescence spectra of **C-EP1**, **C-EP2**, **C-EP5**, and **C-EP6** are shown in Figure 8, and their emission peak maxima, Stokes shifts, and quantum yields relative to ZnTPP (Φ_F = 0.038 in pyridine)[18] are listed in Table 1. The fluorescence quantum yield of **C-EP1** (9.3%) is slightly higher than that of **Zn-EP** (8.3%), and its Stokes shift is smaller (112 cm^{-1} for **C-EP1** and 235 cm^{-1} for **Zn-EP**), indicating that the dimer provides a more rigid structure and raises the fluorescence

(16) Kasha, M. *Radiat. Res.* **1963**, *20*, 55−70.
(17) (a) Arnold, D. P.; James, D. A. *J. Org. Chem.* **1997**, *62*, 3460−3469. (b) Shultz, D. A.; Lee, H.; Kumar, R. K.; Gwaltney, K. P. *J. Org. Chem.* **1999**, *64*, 9124−9136.
(18) Ambroise, A.; Li, J.; Yu, L.; Lindsey, J. S. *Org. Lett.* **2000**, *2*, 2563−2566.

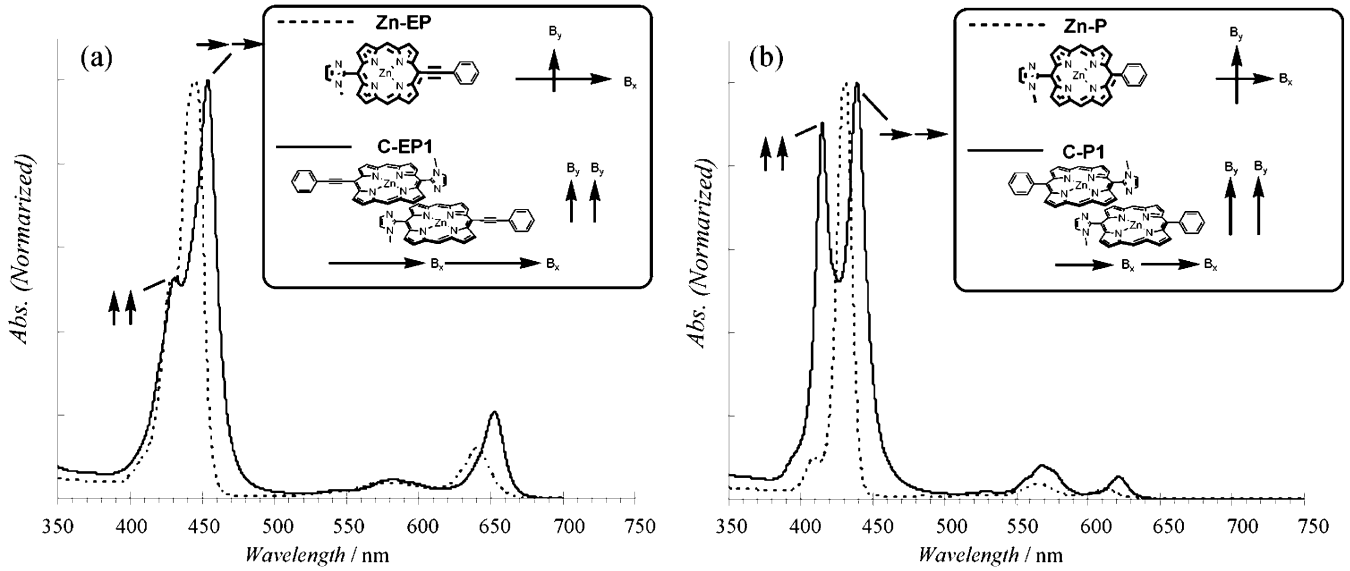

Figure 5. UV−vis absorption spectra in pyridine of (a) **Zn-EP** (dashed line) and **C-EP1** (solid line) and (b) **Zn-P** (dashed line) and **C-P1** (solid line). Inset: schematic dipole directions and dipole−dipole coupling.

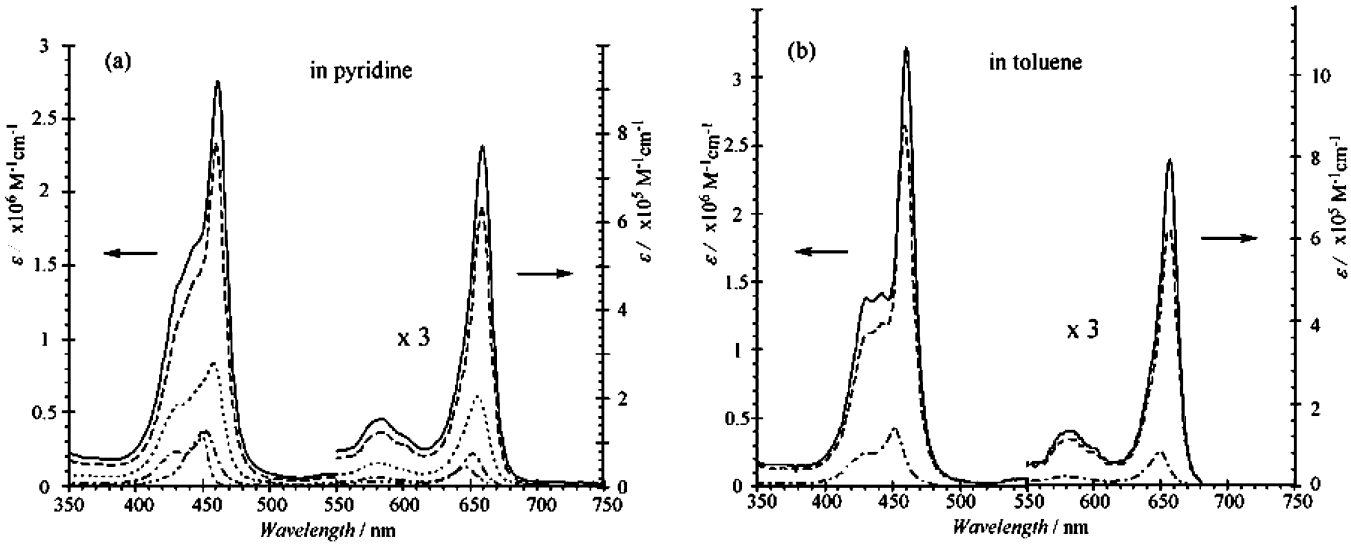

Figure 6. UV−vis absorption spectra (a) in pyridine and (b) in toluene. In (a), **Zn-EP-Zn**, **C-EP1**, **C-EP2**, **C-EP5**, and **C-EP6** (from the bottom to the top). In (b), **Zn-EP**, **N-EP5**, and **N-EP6** (from the bottom to the top).

intensity compared to **Zn-EP**, though the vibrational degree of freedom increased. In general, increasing the aggregation number tends to decrease the fluorescence quantum yield. In this case, however, the increase in the number of dimer units (two for **C-EP2**, five for **C-EP5**, and six for **C-EP6**) does not reduce the fluorescence quantum yields either, satisfying an important prerequisite for LH antennae. If anything, the yield increases along with increasing the number of dimer units.

Because of the inherently high fluorescence quantum yield of **Zn-EP** (8.3%), as compared with those of zinc(II) porphyrin substituted by *meso*-tetraaryl and alkyl groups (normally $\Phi_F = 3-4\%$), macrocyclic **C-EP5** and **C-EP6** exhibit the highest class of fluorescence quantum yields as porphyrin arrays.

The steady-state fluorescence excitation anisotropy (FEA) spectra in pyridine were recorded at 670 nm to obtain information on the relative orientation between absorption and emission transition dipole moments (Figure 9). The steady-state FEA spectra showed negative anisotropy values (r) in the high energy Soret band and positive values at the low energy Soret and Q-bands for all four molecular systems.[3b,7a,11,19] It should be noted that the absolute r values are smaller in **C-EP5** and **C-EP6** compared to **C-EP1** and **C-EP2**, indicating the existence of additional depolarization channels in the cyclic assembly systems. Assuming that the magnitudes of r values originate mainly from the depolarization processes by the rotational diffusion motion in solution, the cyclic molecular systems should have larger r values than those of the reference molecules **C-EP1** and **C-EP2** because of their larger hydrodynamic volumes.[7a,20] Thus, the relatively small r values in cyclic systems imply the involvement of another depolarization channel, such as the redistribution of transition dipoles by the excitation energy hopping process.[19]

Fluorescence Lifetime and Anisotropy Decay. The time-resolved fluorescence decays were measured at several wavelengths in pyridine by a time-correlated single-photon-counting

(19) Osuka, A.; Kim, D.; et al. *J. Phys. Chem. B* **2005**, *109*, 11223−11230.
(20) Lakowicz, J. R. *Principles of Fluorescence Spectroscopy*, 2nd ed.; Kluwer Academic/Plenum Publishers: New York, 1999.

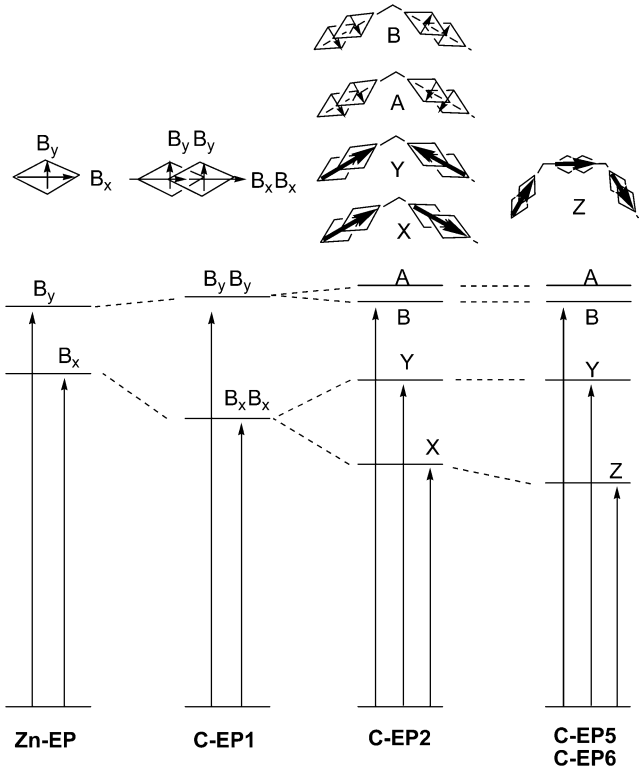

Figure 7. Excitonic dipole−dipole coupling within **C-EP1**, **C-EP2**, **C-EP5**, and **C-EP6**.

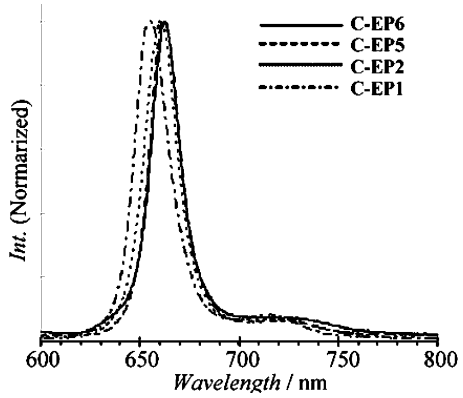

Figure 8. Fluorescence spectra of **C-EP1**, **C-EP2**, **C-EP5**, and **C-EP6** in pyridine.

(TCSPC) technique at the magic angle, and their fitted parameters are listed in Table 1. The fluorescence lifetimes are shortened slightly in the order **C-EP1** > **C-EP2** > **C-EP5** > **C-EP6**. The fluorescence quantum yields increase in the same order. Therefore, these results indicate that the radiative decay rate k_F increases relative to the other decay rates as the number of ring components increases. The Stokes shifts also decrease slightly from 92 cm^{-1} (**C-EP5**) to 88 cm^{-1} (**C-EP6**), indicating that the structural difference between ground and excited states decreases by forming cyclic pentamers and hexamers. This trend is more evident in **N-EP5** and **N-EP6** in toluene. The faster k_F and smaller Stokes shift of **EP6** seem to be correlated.

The fluorescence anisotropy decays of **C-EP1** and **C-EP2** were fitted with the time constants of 1.07 and 2.73 ns, respectively, representing the rotational correlation times (Figure 11). In the case of **C-EP5** and **C-EP6**, on the other hand, the temporal profiles were fitted with the biexponential function,

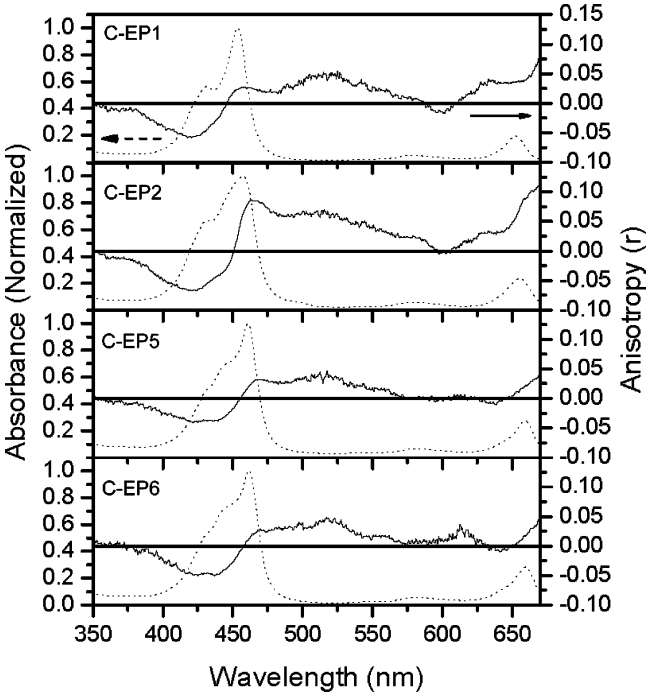

Figure 9. Steady-state fluorescence excitation anisotropy spectra of **C-EP1**, **C-EP2**, **C-EP5**, and **C-EP6** in pyridine recorded at 670 nm. The polarized excitation spectra (I_{VV} and I_{VH}) were measured and calculated by $r = (I_{VV} - GI_{VH})/(I_{VV} + 2GI_{VH})$.

Table 2. Fluorescence Excitation Anisotropy (*r*) and Anisotropy Decay Time (Φ)[a]

sample	r_{max}[b]	r_{min}[c]	Φ[d]/ns
C-EP1	0.04	−0.06	1.03
C-EP2	0.09	−0.07	2.73
C-EP5	0.03	−0.04	
C-EP6	0.03	−0.05	

[a] All the experiments were performed in pyridine. [b] The maxima anisotropy values around Soret bands. (Figure 9). [c] The minima anisotropy values around Soret bands (Figure 9). [d] The $\lambda_{ex} = 420$ nm and $\lambda_{em} = 650$ nm were applied for the anisotropic fluorescence measurement (Figure 11). The anisotropy decay times were obtained by averaging the fitted parameters measured in several emission wavelengths.

which showed a time constant of less than ∼40 ps and much longer (>10 ns). Because of the large hydrodynamic volumes of **C-EP5** and **C-EP6**, the fast depolarization component (∼40 ps) could not be assigned to rotational diffusion processes. Instead, they were assigned to other depolarization channels, such as energy migration or transition dipole redistribution processes. Thus, we conjecture that the EEH processes in **C-EP5** and **C-EP6** occur in a few tens of picoseconds.

Isotropic and Anisotropic Transient Absorption Measurement. To investigate the EEH processes occurring in **C-EP5** and **C-EP6**, we measured femtosecond transient absorption (TA) decay with pump power dependence as well as transient absorption anisotropy (TAA) changes. We tuned the excitation wavelength for the Q-band ($\lambda_{pump} = 650$ nm) because the Q-band excitation could eliminate complicated processes arising from the involvement of the internal conversion process from the S_2 to S_1 state.

The transient absorption decays corresponding to the induced absorption signal were measured at the magic angle (Figure 12). The fitted parameters and the pump power conditions are summarized in Table 3.

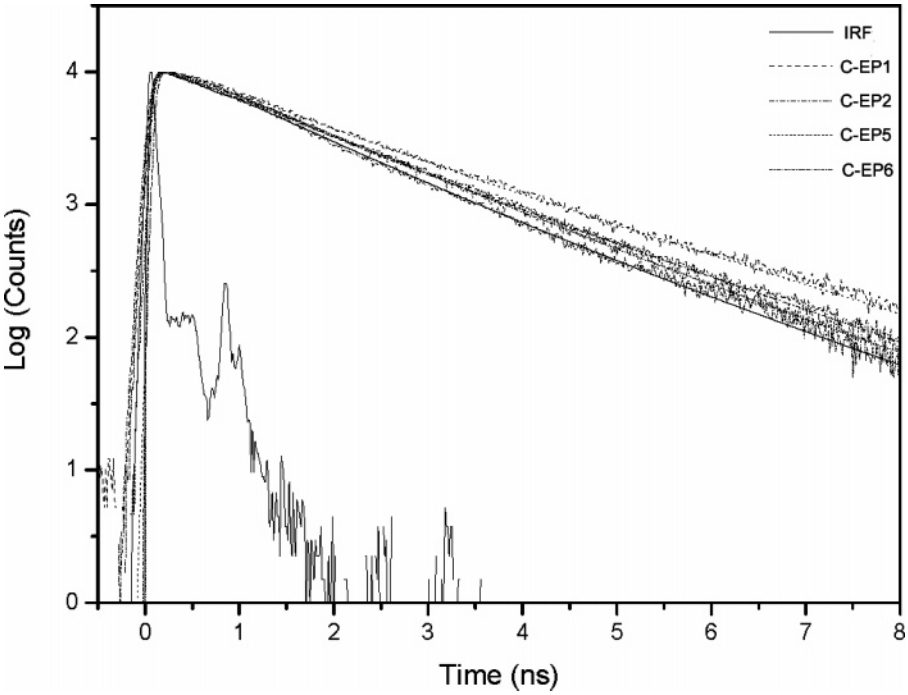

Figure 10. Time-resolved fluorescence decay profiles of **C-EP1**, **C-EP2**, **C-EP5**, and **C-EP6** in pyridine, where the excitation and the emission wavelengths were 420 and 670 nm, respectively. Instrumental response function (IRF) of our TCSPC system was ~60 ps.

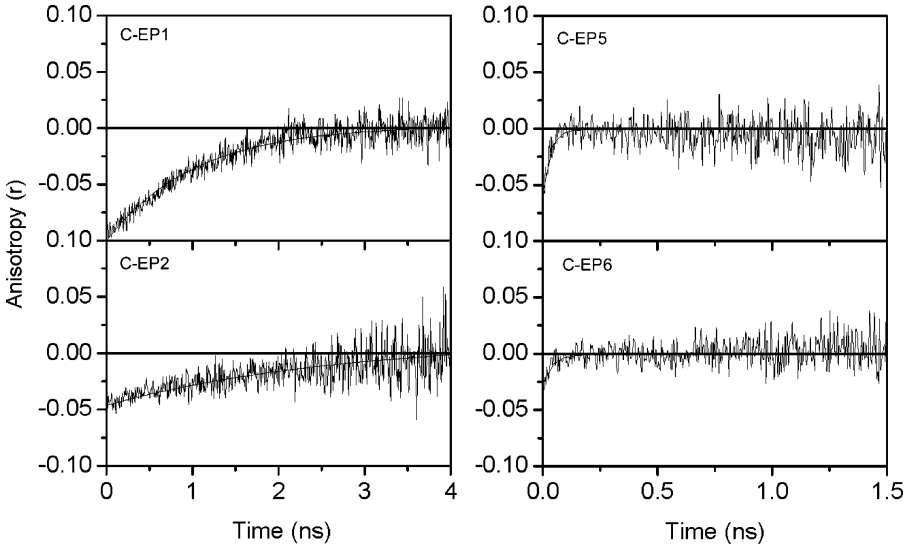

Figure 11. Time-resolved fluorescence anisotropy decay profiles of **C-EP1**, **C-EP2**, **C-EP5**, and **C-EP6** in pyridine, where the excitation and the emission wavelengths were the same as those of the experiment of magic angle fluorescence decay. The polarized excitation spectra (I_{VV} and I_{VH}) were measured, and the time-resolved anisotropy decay r(t) was calculated by $r(t) = \{I_{VV}(t) - GI_{VH}(t)\}/\{I_{VV}(t) + 2GI_{VH}(t)\}$.

C-EP1 showed no pump power dependence as the intensity of the pump pulse was varied from high (1.8 mW) to low (0.3 mW). In contrast, when **C-EP2** was excited by high pump power, two fast decay components (0.48 and 14 ps) and a slow decay component (1.45 ns) were observed, though no fast component was observed under low power conditions, where the time constant of the slow decay component was fixed according to the TCSPC data.[7] In **C-EP5** and **C-EP6**, one slow and two fast decay components were observed even under low pump power conditions. The amplitudes of the two fast components became dominant under high power conditions, i.e., 58% and 50% for **C-EP5** and **C-EP6**, respectively. Notably, the amplitudes of the medium component in **C-EP5** (22 ps) and **C-EP6** (19 ps) increased as the pump power increased from 0.3 to 1.8 mW. These time constants were considered to represent the S_1-S_1 exciton−exciton annihilation processes, since they become manifest only under high pump power conditions. The fastest components (1−2 ps) observed for **C-EP5** and **C-EP6** are expected to be associated with higher order annihilation processes, which could be observed in multichromophoric systems, especially when the samples are excited by high pump power pulses.

At the same pump/probe wavelengths, the transient absorption anisotropy (TAA) decay profiles were obtained under low pump power conditions to avoid multiexciton processes observed in the power dependence experiments (Figure 13). The fitted parameters are listed in Table 4. In **C-EP1**, the anisotropy decay was fitted with a fast (~300 fs) and a slow (~1 ns) decay

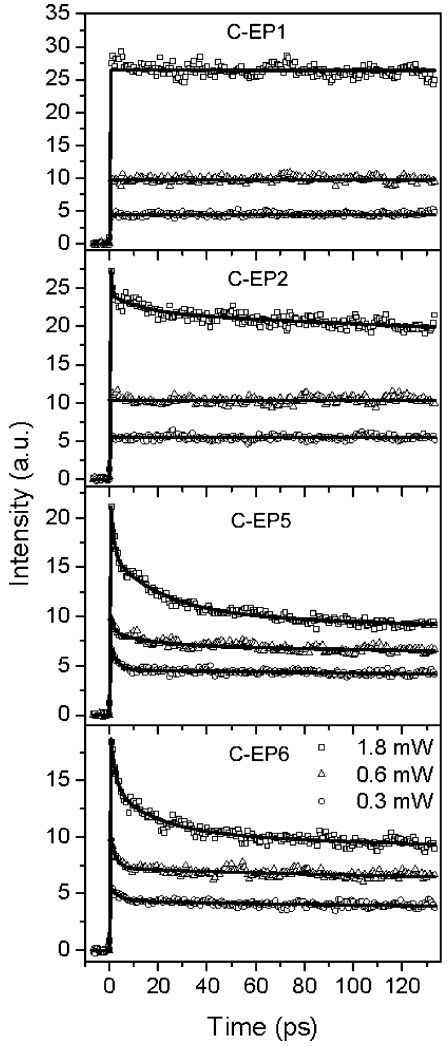

Figure 12. Transient absorption decay profiles of **C-EP1**, **C-EP2**, **C-EP5**, and **C-EP6** (from top to bottom) in pyridine including power dependence, where the pump and probe wavelengths are 650 and 520 nm.

component in a short time window (13 ps). The observed fast decay component (~300 fs) was similar to that of the dimer (200 fs),[11] which was assigned to both the intrachromophoric dipole equilibrium and the interchromophoric EEH process within the dimer. The steady-state absorption spectral shapes of **C-EP1** differ significantly from those of **C-P1** with the introduction of the ethynyl moiety. A much higher oscillator strength was observed for the B_x component as compared to B_y. The uneven transition dipoles may suppress the exchange rate significantly. In addition, the slow component (~1 ns) is consistent with the anisotropy decay observed in the TCSPC experiment and is assigned to the rotational correlation time.

In contrast to **C-EP1**, three decay components were observed for **C-EP2**, **C-EP5**, and **C-EP6**. The slowest component in **C-EP2** was fitted to 2.7 ns, which is in accordance with the anisotropy decay observed in TCSPC, and those in **C-EP5** and **C-EP6** (>5 ns) could not be assigned exactly but are expected to be associated with the rotational correlation times. Besides the fastest time constant (~300 fs), which could be explained in the same manner as the case of **C-EP1**, newly observed picosecond components (4−5 ps) most likely represent additional depolarization channels due to the excitation energy migration processes along the entire cyclic array.

Table 3. Transient Absorption Decay Time Constants at Magic Angle[a] with Pump Power Dependence of **C-EP1**, **C-EP2**, **C-EP5**, and **C-EP6** in Pyridine

sample	power[b]	τ_1	τ_2	τ_3
C-EP1				1.65 ns
	1.8 mW			100%
	0.6 mW			100%
	0.3 mW			100%
C-EP2		0.5 ps	14 ps	1.45 ns
	1.8 mW	31%	7%	62%
	0.6 mW			100%
	0.3 mW			100%
C-EP5		1.3 ps	22 ps	1.42 ns
	1.8 mW	32%	26%	42%
	0.6 mW	24%	11%	65%
	0.3 mW	43%	3%	54%
C-EP6		2.0 ps	19 ps	1.38 ns
	1.8 mW	29%	21%	50%
	0.6 mW	32%	2%	66%
	0.3 mW	24%	5%	71%

[a] The λ_{pump}=650 nm and λ_{probe}=520 nm were applied for the transient absorption measurement. [b] The pump energy per pulse was 360, 120, and 60 nJ for 1.8, 0.6, and 0.3 mW, respectively, because the repetition rate of 5 kHz was applied.

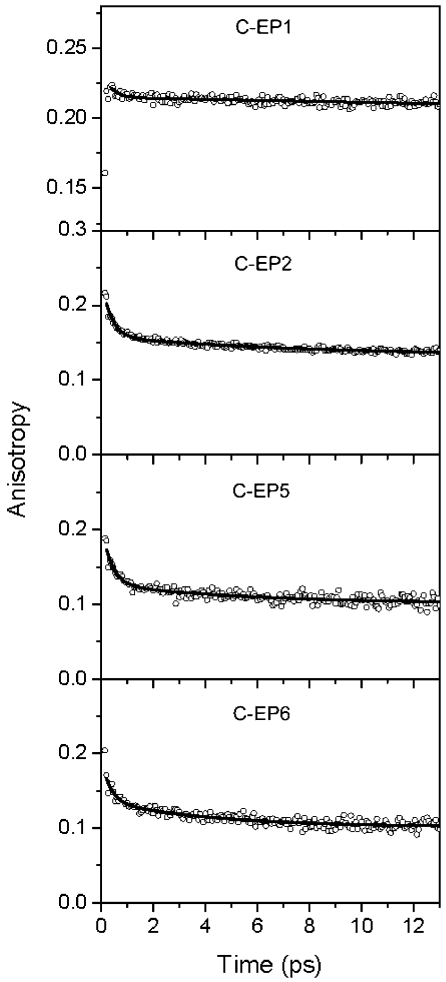

Figure 13. Transient absorption anisotropy decay profiles of **C-EP1**, **C-EP2**, **C-EP5**, and **C-EP6** (from top to bottom) in pyridine, where the pump and probe wavelengths are 650 and 520 nm.

In circularly arranged multichromophoric systems, the EEH times can be analyzed explicitly by simultaneous consideration

Table 4. Transient Absorption Anisotropy Decay Time Constants of **C-EP1**, **C-EP2**, **C-EP5**, and **C-EP6** in Pyridine[a]

sample	τ_1 (%)	τ_2 (%)	τ_3 (%)	r_∞
C-EP1	0.3 ps (4%)		1.03 ns (96%)	0.20
C-EP2	0.27 ps (35%)	4.3 ps (10%)	2.70 ns (55%)	0.14
C-EP5	0.36 ps (39%)	5.4 ps (13%)	5 ns < (48%)	0.10
C-EP6	0.33 ps (29%)	4.2 ps (18%)	5 ns < (53%)	0.10

[a] The λ_{pump} = 650 nm and λ_{probe} = 520 nm were applied for the measurement. The anisotropy decay profiles were obtained under a low pump power condition (0.3 mW).

of the two time constants, τ_{ann} and τ_{dep}. Although neither exciton−exciton annihilation nor anisotropy depolarization directly represents the EEH times between the energy hopping units, the EEH times can be determined by synchronizing the two time constants by modeling the EEH mechanism.

Discussion

EEH Models in Cyclic Pentamer and Hexamer Arrays. We have analyzed the EEH processes of **C-EP5** and **C-EP6** using the S_1-S_1 exciton−exciton annihilation and anisotropy depolarization processes on the basis of Fleming's method.[21] Assuming migration-limited annihilation and a random-walk formalism of anisotropy decay, where the dimer unit can act as a coherent domain within the strong coupling limit, the EEH time can be obtained from the analytical depolarization and exciton−exciton annihilation times using eqs 1 and 2, where N is the number of excitation energy hopping sites, α, the angle between the neighboring transition dipoles (108° for **C-EP5** and 120° for **C-EP6**), τ_{ann}, the slowest exciton−exciton annihilation time, τ_{dep}, the depolarization time, and $\tau_{hopping}$, the inverse of the nearest neighbor energy hopping rate:[21]

$$\tau_{dep} = \frac{\tau_{hopping}}{4(1-\cos^2(2\pi/N))} = \frac{\tau_{hopping}}{4(1-\cos^2\alpha)} \quad (1)$$

$$\tau_{ann} = \frac{N^2-1}{24}\tau_{hopping} \quad (2)$$

where τ_{dep} and τ_{ann} were obtained from, respectively, TAA and transient absorption decay depending on the pump power. For **C-EP5** where $N = 5$, we substituted τ_{dep} = 5.4 ps in eq 1 and obtained $\tau_{hopping}$ = 19.5 ps, and in a different approach, the substitution of τ_{ann} = 22 ps in eq 2 gave $\tau_{hopping}$ = 22 ps. Similarly, for **C-EP6** where $N = 6$, we substituted τ_{dep} = 4.2 ps in eq 1 and obtained $\tau_{hopping}$ = 12.6 ps for **C-EP6** and substituted τ_{ann} = 19 ps in eq 2 and obtained $\tau_{hopping}$ = 13 ps. Interestingly, the two different experimental observables, τ_{dep} and τ_{ann}, result in consistent EEH times ($\tau_{hopping}$) within small deviations. Thus, the excitation energy migration processes in these macrocyclic arrays can be well demonstrated by a Förster-type incoherent energy hopping model. By taking an average value, we determined the EEH times between the nearest neighboring dimer units to be 21 ± 1 ps for **C-EP5** and 12.8 ± 0.2 ps for **C-EP6**. In our previous study,[11] the same method has been applied to the EEH times for **C-P5** and **C-P6** to determine the EEH times of ∼8.0 and ∼5.3 ps, respectively. A difference in the EEH rates will be discussed in the next section.

Transition Dipole Coupling Energy and EEH Times in Cyclic Array Systems. As described in the previous section, the EEH times of larger ring systems (**C-EP5** and **C-EP6**) are longer than those of smaller ring systems (**C-P5** and **C-P6**), and considering the molecular size, the EEH times of pentagonal structures (**C-EP5** and **C-P5**) are longer than their corresponding hexagonal structures (**C-EP6** and **C-P6**). Naturally, one would expect that the larger distance between chromophores would lead to shorter EEH times in cyclic array systems as well because both through-bond and through-space energy transfer rates strongly depend on the center-to-center distances proportional to R^{-6} and $\exp^{-R}$, respectively. However, the shorter EEH times in hexagonal structures as compared to those in pentagonal structures are still questionable. This seems to stem from the fact that the angle 120° of the 1,3-bis(ethynyl)phenylene linker is better suited for hexagonal structures than it is for pentagonal ones.

In this regard, the faster EEH times in hexagonal structures are thought to arise from the difference in the relative orientation between the nearest neighboring chromophores. As seen in the Förster-type energy transfer rate (eq 3) and the dipole coupling formula (eq 4), the orientation factor (κ) is in the numerator in both equations:

$$k_{TS} = \frac{8.8\times10^{-25}\,\kappa^2\,\Phi}{n^4R^6\tau}J \quad (3)$$

$$V_{ij} = \frac{5.04\,f_L^2|\vec{\mu}_i||\vec{\mu}_j|\kappa}{\epsilon_{op}R_{TS}^3} \quad (4)$$

where n is the refractive index of the solvent, R, the center-to-center distance between donor and acceptor, τ, the fluorescence lifetime of an energy donor, κ, the orientation factor, Φ, the fluorescence quantum yield, J, the spectral overlap integral in eq 3; V_{ij} is the transition dipole coupling energy, f_L, the Lorenz local field correction factor ($f_L = (\epsilon_{op}+2)/3$), ϵ_{op}, the dielectric constant at optical frequencies, $\mu_{i,j}$, the transition dipole moment, and R_{TS}, the center-to-center distance in nm, in which the subscript TS means through-space in eq 4.[22] The orientation factor κ is calculated by eq 5:

$$\kappa^2 = (\cos\theta_T - 3\cos\theta_i\cos\theta_j)^2 \quad (5)$$

where θ_T is the dihedral angle between the two transition dipole moments, and θ_i and θ_j are the angles between these dipoles and the segment joining the two transition dipole moments.

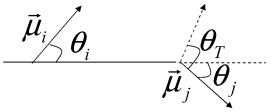

On the assumption of perfect planar pentagonal and hexagonal structures, κ is calculated to be 1.65 for **C-EP5** and 1.75 for **C-EP6**.[23] The difference in κ seems small, but when the EEH processes occur from one hopping unit to the other one continuously, the effect of the small deviation in κ would increase exponentially. In summary, the larger value of κ in hexagonal structures induces a larger transition dipole coupling

(21) Bradforth, S. E.; Jimenez, R.; van Mourik, F.; van Grondelle, R.; Fleming, G. R. *J. Phys. Chem.* **1995**, *99*, 16179−16191.

(22) Morandeira, A.; Vauthey, E.; Schuwey, A.; Gossauer, A. *J. Phys. Chem. A* **2004**, *108*, 5741−5751.

(23) The angular parameters (θ_T, θ_i, and θ_j) values used for estimating κ are 72°, 36°, and 36°, respectively, for **C-EP5**, and 60°, 30°, and 30°, respectively, for **C-EP6**.

energy as compared to that in pentagonal structures, resulting in shorter EEH times in hexagonal structures. That is, well-oriented hexagonal arrays by the combinative conformation of chromophores and linkers exhibit faster EEH processes than pentagonal arrays. Thus, the difference between the experimentally deduced EEH times of **C-EP5** and **C-EP6** is mainly accounted for by the orientation factor induced by the conformational differences. Indeed, the slightly more well-resolved Soret bands and red-shifted Q-bands of **C-EP6** as compared with those of **C-EP5** support our arguments.

Assessment of Antenna Functions and Outlook. The EEH time constants for **C-EP5** (21 ps) and for **C-EP6** (12.8 ps) are small enough compared with the lifetimes for **C-EP5** (1.42 ns) and **C-EP6** (1.38 ns). In addition to their fluorescence intensities, which are even larger than that of a monomeric unit, macrocyclic arrays are regarded as excellent LH antennae. Different EEH times between **C-EP5** and **C-EP6** indicate that EEH times depend strongly on the orientation factor of the constituent elements of macrocyclic arrays. However, the present study only investigated pentagonal and hexagonal macrocyclic arrays. The hypothesis should be confirmed for macrocycles larger than hexagonal arrays.

Comparison of the present EEH times with those of smaller macrocycles, **C-P5** (∼8.0 ps) and **C-P6** (∼5.3 ps), suggest that the EEH time is dependent on the center-to-center distance between the coherent dimers. Coplanarity and electronic communication through the ethyne bond in **C-EP5** and **C-EP6** does not appreciably accelerate the EEH times.

Introduction of the ethyne moiety between porphyrin and phenylene causes the red-shifted absorption spectra of **C-EP5** and **C-EP6** compared to **C-P5** and **C-P6**. In addition, the Q(0,0) band of **C-EP5** and **C-EP6** increases considerably. These features are suitable as a second antenna into which excited energy flows from a peripheral higher energy antenna. Inspection of the overlap between the emission spectra of **C-P5** and **C-P6** and absorption spectra of **C-EP5** and **C-EP6** suggests that their composites provide an efficient energy cascade system like LH2 and LH1.

Conclusions

We have demonstrated the effective synthesis of the macrocyclic porphyrin arrays **EP5** and **EP6** by complementary coordination of *m*-bis(ethynylene)phenylene-linked imidazolylporphyrin **Zn-EP-Zn**. The proton NMR spectra of **N-EP5** and **N-EP6** indicate fast rotation of the porphyrin moieties along the ethyne axis. The covalently linked macrocyclic porphyrin arrays **C-EP5** and **C-EP6** were confirmed by mass spectrometry and analyzed by various steady-state and time-resolved photophysical measurements in pyridine. Electronic and excitonic dipole−dipole couplings in **EP5** and **EP6** macrocycles were examined by comparison with various reference porphyrins. Introduction of the ethyne moiety induces a large transition dipole along the ethyne axis (B_x) and lowers the energy level of the Q(0,0) band. Excitonic dipole−dipole coupling directed toward B_x was dominant, whereas that toward B_y was negligible.

Based on the exciton−exciton annihilation and anisotropy depolarization times, we have determined the EEH times in cyclic multichromophoric systems to be 21 ps for **C-EP5** and 12.8 ps for **C-EP6**. It is notable that the EEH times obtained by the two methods closely match each other. The hexagonal macrocyclic arrays with a better orientation of transition dipoles afforded a shorter EEH time compared to pentagonal arrays. This is a new finding for synthetic macrocyclic antennae.

Experimental Section

All of the synthetic procedures and photophysical experiments are described in the Supporting Information.

Acknowledgment. This work was supported by Grant-in-Aids for Scientific Research (A) (Y.K.), Young Scientists (B) (A.S.), Scientific Research on Priority Areas (No. 15036248), Reaction Control of Dynamic Complexes (Y.K.) from the Ministry of Education, Culture, Sports, Science and Technology, Japan and JSPS (Japan Society for the Promotion of Science), and the National Creative Research Initiatives Program of the Korea Science and Engineering Foundation of Korea (D.K.).

Supporting Information Available: Synthetic procedures, photophysical experiments; GPC analyses of **C-EP1**, **C-EP2**, **EP5**, and **EP6**; MALDI-TOF mass spectra of **C-EP1**, **C-EP2**, **C-EP5**, and **C-EP6**; 2D NMR spectrum of **N-EP5**; temperature-variable ^{1}H NMR spectra of **N-EP5**; UV−vis spectra of all porphyrins in toluene and pyridine, and complete refs 11 and 19. This material is available free of charge via the Internet at http://pubs.acs.org.

JA0583214